Mass Transfer Mechanism Within Commercial PTFE Membranes In Spacer-Filled Direct Contact Membrane Distillation

Quoc Linh Ve[1*], Minh Cuong Do[2], Thanh Cuong Nguyen[3], Quoc Huy Nguyen[4], Quang Lich Nguyen[5], Minh Tuan Hoang[6], Farzaneh Mahmoudi[7]

[1,2,3,4] *Faculty of Engineering and Food Technology, University of Agriculture and Forestry, Hue University, Thua Thien Hue 530000, Vietnam; vqlinh@hueuni.edu.vn*

[5] *School of Engineering and Technology, Hue University, Thua Thien Hue 530000, Vietnam*

[6] *Faculty of Thermal Refrigeration Engineering, Hue Industrial College, 70 Nguyen Hue, Thua Thien Hue 530000, Vietnam*

[7] *The Commonwealth Scientific and Industrial Research Organisation (CSIRO), Private Bag 10, Clayton South, VIC, 3169, Australia*

Abstract: The mass transfer mechanism within commercial PTFE membrane with various nominal pore sizes in spacer-filled direct contact membrane distillation (DCMD) was determined. Mass fluxes and membrane permeability (MP) values for each commercial PTFE membrane were experimentally measured. The MP values increased insignificantly with 2.3% and 4% when the inlet temperature at feed side rose from 40^0C to 50^0C in different membrane pore sizes. All investigated mass transfer models except from Dusty Gas model were good enough to simulate the mass transfer inside smaller membrane pore sizes (0.22 µm, and 0.45 µm). Compared to combined diffusion model, the predicted mass fluxes using the overall mass transfer model including the contribution of Poiseuille flow obtained better agreement with experimental results for larger membrane pore size (1 µm). The mean absolute percentage error (MAPE) values for combined diffusion model were up to 16.5% compared with the Ding et al. model or Schofield et al. model (under 3%). Regarding the root mean square error (RMSE), the combined diffusion model obtains larger values than the mass transfer model considering the Poiseuille flow contribution. Consequently, the contribution of Poiseuille flow in mass transfer mechanism within smaller PTFE membrane pores (0.22 µm, and 0.45 µm) could be ignored, however, the contribution of Poiseuille flow to the overall mass transfer should be included in case of larger membrane pores (1 µm), or the case of applied transmembrane hydrostatic pressure.

Keywords: Direct Contact Membrane Distillation, Mass Transfer Within Membrane Pores, Membrane Permeability

1. INTRODUCTION

Membrane distillation (MD) is one of conventional separation technologies. It is a thermally driven process and uses the hydrophobic microporous membranes for not only non-volatile matters separation from saline solution to produce freshwater [1], but also volatile compounds extraction from water or wastewater by air gap membrane distillation (AGMD), vacuum membrane distillation (VMD), or sweeping gas membrane distillation [2-5]. Direct contact membrane distillation (DCMD) is one of the most implemented popular configurations in desalination sector. In DCMD, both feed solution and permeate solution are kept in contact directly with hydrophobic membrane [1].

When dealing with membrane features and performance in the context of Membrane Distillation (MD) technologies, several critical factors need to be considered. These encompass a comprehensive investigation into how water molecules traverse the intricate pore structures of membranes, an evaluation of the tortuosity parameter within these membrane pores, and a comprehensive understanding of various parameters influencing the diffusion process, particularly considering the diminishing momentum of vapour molecules [6].

Different models and simulated methods have been used to investigate the mass transfer property within the MD membrane pores, such as the Fick's law model, Ballistic transport model, the dusty gas model, structural network models, and Schofield's model [7, 8]. The different approaches have their benefits and drawbacks. Fick’s law model was one of the simplest approaches to simulate the mass transfer in membrane region. Nevertheless, the membrane structure like the pore size, the porosity, and the tortuosity were not considered [7]. To Ballistic transport model, the flux prediction for all of the membranes was not accurate and the difference between measured and predicted mass

flux could reach up to 73% in some cases [7]. Schofield's model ignored the effect of pore size distribution and only took into account the average pore size in mass transfer simulation [7]. Amongst mass transfer models, the dusty gas model is the most common one implemented in examining mass transfer [9]. In the dusty gas model [10], both a diffusion mechanism including Knudsen, molecular, and surface diffusion [11] and Poiseuille flow [11-13] should be taken into account in the mass transfer through the hydrophobic membrane . However, the surface diffusion and Poiseuille flow are not mentioned in most cases because of their insignificant contribution to the mass transport process [14]. Dahiru et al. [15] developed Matlab codes to predict DCMD mass fluxes based on experimental works from Cath et al. [16] and Andrjesdóttir et al. [17]. In this study, the Poiseuille flow was not mentioned in their predicting models including large pore size of membrane case (1.2 µm). Consequently, transition model (Knudsen – Molecular diffusion) was the most appropriate prediction model in case of the effect of operating parameters (feed temperature, feed flow rate, and permeate temperature) and membrane pore size. However, according to Ding et al. [6] and Damtie et al. [18], the impact of Poiseuille flow could be ignored in case of small nominal pore size of membrane (PTFE, 0.1 µm). Otherwise, the role of Poiseuille flow should be mentioned in mass transfer model in case of larger nominal pore size of membrane (PTFE, 0.3 µm; PVDF, 0.2 µm; PVDF, 0.45 µm). As a result, Knudsen diffusion-molecular diffusion-Poiseuille flow transition (KMPT) model in which Poiseuille flow was parallel with the combination flow model between Knudsen and molecular diffusion was proposed to predict mass flux in DCMD configuration [6]. Damtie et al. [18] confirmed that the Poiseuille flow contributed more significant while the Knudsen diffusion decreased in case of increasing feed temperature. Furthermore, the flowrate had an insignificant influence on the Poiseuille mass transfer coefficient. In other studies, the Knudsen-Poiseuille transition model was used to predict mass flux in flat-sheet DCMD in case of deaeration (low pressure of air within membrane pores) for 0.45 µm PVDF membrane and 0.2 µm PP membrane. If the process solutions have not been degassed, the viscous flux could be neglected in mass transfer model [12, 13]. According to [19], the mass transfer within membrane pores depended on the pore size. If the nominal pore size was larger than 2 µm, the molecular diffusion, the Poiseuille flow, or the Poiseuille – molecular diffusion combination was responsible for the mass transfer mechanism within the membrane pores. The dominant mechanism of mass transfer is Knudsen diffusion when the nominal pore size of membrane is 0.01 µm [8]. From many studies [20-24], the used membranes had the nominal pore size in the range of 0.1 µm – 1 µm, therefore the calculated Knudsen number was from 0.1 to 1. As a result, the Knudsen-molecular diffusion transition form was dominant mass transfer mechanism in the mass flux prediction of DCMD configuration [23-25]. Four selective mass transfer models through membrane pores are illustrated in Figure 1.

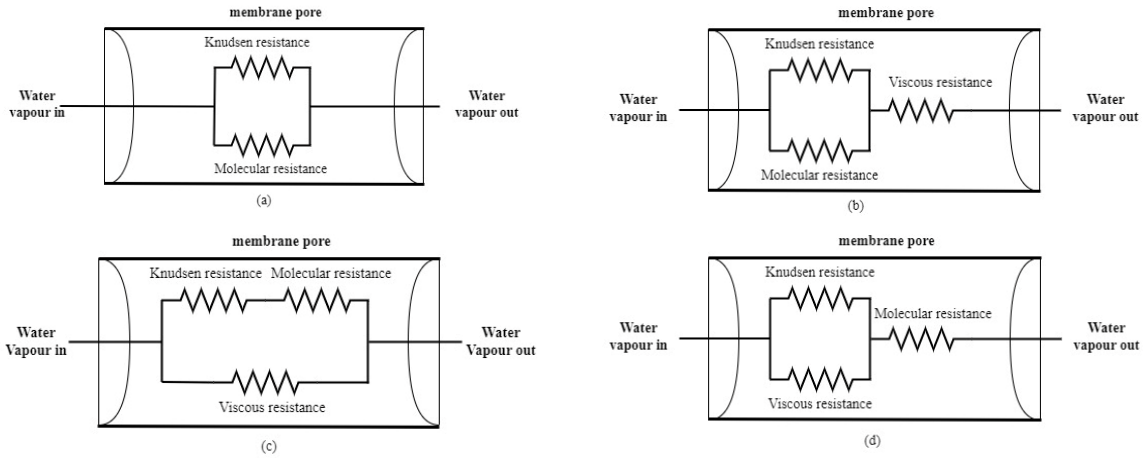

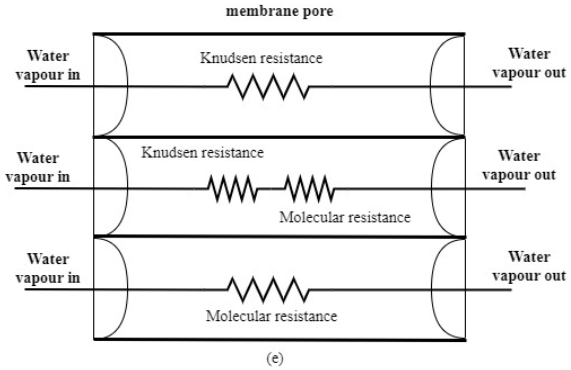

Figure 1. Electrical analogue of different models for predicting MD membrane mass transfer coefficient: (a) Combined diffusion model [26]; (b) Ding et al. model [6]; (c) Dusty gas model [27] ; (d) Schofield et al. model [13] ; (e) Phattaranawik et al. model [28]

Consequently, there has not been a consistent determination in selecting the most appropriate mass transfer mechanism within membrane pores amongst existing studies. This study aims to determine the influence level of viscous flow (or Poiseuille flow) on the overall mass transfer mechanism within different membrane pore size (0.22 μm – 0.45 μm – 1 μm) through analysing the mass transfer correlations in existing studies in comparison with experimental results. To confirm the best agreement between experimental and modelling results, the root mean square error (RMSE) and mean absolute percentage error (MAPE) are used [29-32].

2. THEORY

2.1. Heat Transfer

Direct contact membrane distillation is a complex process involving both heat and mass transfer, as illustrated in Figure 2. To begin with, the convective heat is transferred across the liquid boundary layer to the feed membrane surface. Next, heat in form of conduction heat and vapour latent heat passes through membrane pores. Finally, the convective heat is removed from membrane surface across the liquid boundary layer in permeate side.

The heat transfer rate across the boundary layer of both the feed side and the permeate side:

$$Q_f = h_f \times A \times (T_f - T_{m,f}) \quad (1)$$

$$Q_p = h_p \times A \times (T_{m,p} - T_p) \quad (2)$$

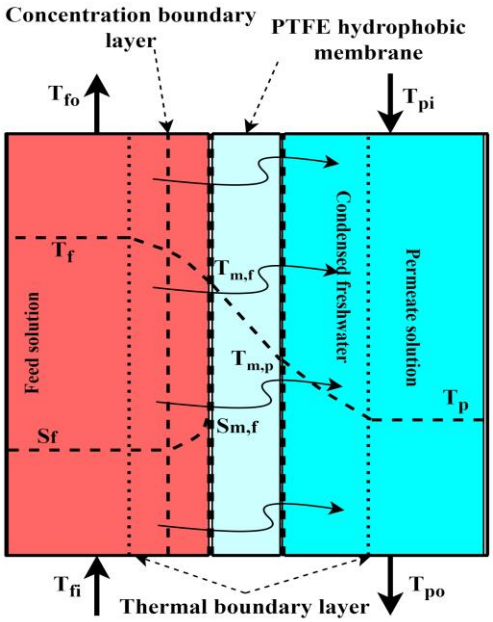

Figure 2. Heat and mass transfer in spacer-filled DCMD module

The heat transfer rate through the membrane can be expressed [11]:

$$Q_m=\frac{k_m}{\delta}\times A\times\left(T_{m,f}-T_{m,p}\right)+J_w\times A\times\Delta H_{v,w} \tag{3}$$

According to [24], amongst different models to predict the thermal conductivity of membrane (k_m), the Type II thermal conductivity model proposed by Maxwell obtained the best agreement between measured and calculated heat transfer rate as well as mass flux, therefore this model is applied in this study, as described below [24, 33]:

$$k_m=\frac{k_g\left[1+2\beta\varphi+\left(2\beta^3-0.1\beta\right)\varphi^2+0.05\varphi^3\exp(4.5\beta)\right]}{1-\beta\varphi}$$

$$\beta=(k_p-k_g)/(k_p+2k_g) \tag{4}$$

$$\varphi=1-\varepsilon_m$$

As mentioned in [11, 33, 34], the thermal conductivity of PTFE ranged from 0.25 $W.m^{-1}.K^{-1}$ to 0.27 $W.m^{-1}.K^{-1}$ at 296K. So, k_g = 0.027 $W.m^{-1}.K^{-1}$ and k_p = 0.27 $W.m^{-1}.K^{-1}$ were assumed to calculate k_m. The porosity of PTFE membrane was 75%.

At the steady state:

$$Q_f=Q_m=Q_p \tag{5}$$

The temperature at the membrane surface in both feed side and permeate side can be derived from Equations (1), (2), (3), (5):

$$T_{m,f}=\frac{h_m\left(T_p+\frac{h_f}{h_p}T_f\right)+h_fT_f-J_w\Delta H_{v,w}}{h_m+h_f\left(1+\frac{h_m}{h_p}\right)} \quad (6)$$

$$T_{m,p}=\frac{h_m\left(T_f+\frac{h_p}{h_f}T_p\right)+h_pT_p+J_w\Delta H_{v,w}}{h_m+h_p\left(1+\frac{h_m}{h_f}\right)} \quad (7)$$

The film heat transfer coefficient (h_f, h_p) can be determined by using a correlation in case of effect of spacer [35, 36]:

$$h_i=0.664k_{dc}\,Re_i^{0.5}\,Pr_i^{0.33}\left(\frac{2d_h}{l_m}\right)^{0.5}\times\frac{k_i}{d_h}$$
$$k_{dc}=1.654\left(\frac{d_f}{t_s}\right)^{-0.039}\varepsilon^{0.75}\left(sin\left(\frac{\theta}{2}\right)\right)^{0.086} \quad (8)$$

In case of using spacer in DCMD module channel, the hydraulic diameter (d_h), and spacer porosity (ε) could be calculated as [35-37].

$$\varepsilon=1-\frac{\pi d_f^2}{2l_mt_s sin\theta} \quad (9)$$

$$d_h=\frac{4\varepsilon}{\left(2(W+t)/Wt+(1-\varepsilon)S_{vsp}\right)}$$
$$S_{vsp}=4/d_f \quad (10)$$

2.2. Mass Transfer Through Membrane Pores

In the DCMD, the mass transfer includes two processes: the volatile component transfers across the boundary layers to the feed-membrane surface, and then passes through the membrane pores. Assuming that measured mass flux is proportional to the vapor pressure difference being the driving force for the mass transfer process, so the mass transfer through membrane itself can be expressed [23, 26, 27, 38, 39]:

$$J_w=C_m\left(p_{v,sf}-p_{v,sp}\right) \quad (11)$$

Where the partial pressures of water vapour being a function of surface temperatures are mentioned in some studies [24, 40].

$$p_{v,si}=\alpha_{wi}\times exp\left(23.238-\frac{3841}{T_{m,i}-45}\right) \quad (12)$$

Where i=f (feed), or i=p (permeate); and αwi is the water activity of solution at feed or permeate side in DCMD module.

To examine the influence of Poiseuille flow in the general mass transfer flow model in membrane pores in case of larger pore size of membrane, the different membrane mass transfer coefficients were investigated, as shown in

Table **1** :

Table 1. Various mass transfer models to predict the membrane mass transfer coefficient through membrane pores

Mass transfer model	*Membrane mass transfer coefficient*	*Notes*
Combined diffusion model [26]	$C_m=\frac{1}{RT_m\delta}\left(\frac{3\tau}{2\varepsilon r}\left(\frac{\pi M}{8RT_m}\right)^{1/2}+\frac{p_a\tau}{M\varepsilon PD}\right)^{-1}$	• *Air is present in membrane pores.* • *No transmembrane hydrostatic pressure [41]*
Ding et al. model [6]	$C_m=\frac{1}{RT_m\delta}\left[\left(\frac{3\tau}{2\varepsilon r}\left(\frac{\pi M}{8RT_m}\right)^{1/2}+\frac{p_a\tau}{\varepsilon PD}\right)^{-1}+0.125\frac{\varepsilon r^2 MP_m}{\tau\mu}\right]$	• *A three-parameter model is developed for larger nominal mean pore diameter (Knudsen diffusion – molecular diffusion - Poiseuille flow transition).*
Schofield et al. model [13]	$C_m=\frac{1}{RT_m\delta}\left[\left(\frac{3\tau}{2\varepsilon r}\left(\frac{\pi M}{8RT_m}\right)^{1/2}+\frac{\tau\mu}{0.125\varepsilon r^2 MP_m}\right)^{-1}+\frac{M\varepsilon PD}{P_a\tau}\right]$	*Considering the effect of Poiseuille flow*
Phattaranawik et al. model [28]	$C_m=\frac{1}{RT_m\delta}\left[\frac{P_a\tau}{M\varepsilon PD}+\frac{3\tau}{2\varepsilon r}\left(\frac{\pi M}{8RT_m}\right)^{1/2}+\frac{1}{\left(\frac{2\varepsilon r}{3\tau}\left(\frac{8RT_m}{\pi M}\right)^{1/2}+\frac{M\varepsilon PD}{P_a\tau}\right)}\right]^{-1}$	*In case of multi-pore size of membrane*
Dusty gas model (DGM) [27]	$C_m=\frac{1}{RT_m\delta}\left[\frac{\mu\tau}{0.125\varepsilon r^2 MP_m}+\frac{1}{\left(\frac{2\varepsilon r}{3\tau}\left(\frac{8RT_m}{\pi M}\right)^{1/2}+\frac{M\varepsilon PD}{P_a\tau}\right)}\right]^{-1}$	*DGM considered the effect of surface diffusion which is neglected in MD process. Knudsen diffusion, molecular diffusion, and Poiseuille flow are mentioned in this model.* *DGM is developed for isothermal system. This model is applied for MD (non-isothermal system) when average temperature across the membrane is assumed (T_m < (20^0C – 53^0C) [41-43]*

The determination of mass transfer through membrane pores in MD depend on Knudsen number (Kn). The Knudsen flow model is dominant when Knudsen number is larger than 1 (Kn>1). If Knudsen number is smaller than 0.01 (Kn < 0.01), molecular diffusion model is the main mass transfer within the membrane pores for all MD configurations except from VMD. For DCMD, when Knudsen number is in the range of (0.01 – 1) or no transmembrane hydrostatic pressure is applied, the combined Knudsen / molecular diffusion flow is dominant mechanism in membrane pores. The Poiseuille model or viscous flow is dominant mechanism when membrane pore size is larger than the mean free path of transported water molecules, and the hydrostatic pressure at transmembrane is applied. For VMD configuration, the operative mechanism is combined Knudsen / viscous flow model when there is a presence of transmembrane hydrostatic pressure, and the Knudsen number is in the transition range (0.01 < Kn < 1). Generally, the interconnectivity of membrane pores is ignored in mass flux prediction in most of MD publications. Therefore, Monte Carlo (MC) simulation models are developed to solve this limitation relating to studying both heat and mass transfer in DCMD [42]. Some empirical models have been developed such as artificial neural network (ANN) or response surface methodology (RSM) to be independent of the determination of mass transport mechanism through MD membrane. These models are used to optimize the MD installations by considering the effect of combination of input operating parameters on given outputs (permeate flux maximization or energy consumption minimization) *[41]*.

For water/air, PD (Pa.m^2/s) is evaluated [11] :

$$PD=1.895\times10^{-5}T_m^{2.072} \quad (13)$$

3. EXPERIMENTAL SET-UP

A lab-scale DCMD apparatus was showed in Figure 3. The flat-sheet membrane module was employed with a treatment area of 225 cm^2 and 4 cm channel height. Plastic spacers were used on both sides of DCMD module to support the membrane and improve the heat transfer. Three kinds of commercially hydrophobic PTFE membranes with different pore sizes (YKF10028, YKF10029, YKF10030) supplied by UNM company, China were used. The nominal pore size diameter of membrane was 0.22 µm (PTFE022), 0.45 µm (PTFE045), 1 µm (PTFE1), respectively. The thickness of all examined membranes is in the range of (180-200) µm. A temperature controller controlled the temperature of feed saline solution in a hot water bath (BE-25L-T). A combination of chiller (CW-5000) and plate heat exchanger was used to cool down the freshwater at permeate side to fixed temperature. Both solutions on hot and

cold side were pumped counter-currently. Temperatures of feed and permeate solutions at the inlet and outlet of DCMD module were measured by four temperature sensor PT100. For collecting experimental data, a data logger (DI-2108) was used. The freshwater production of DCMD system was measured over a time interval and weighed by using a digital scale.

In this study, the feed inlet temperature, T_{fi} was in the range (40^0C – 50^0C) with 5^0C increment, while 20^0C was fixed for the permeate inlet temperature, T_{pi}. The equivalent volume flow rates for both sides of DCMD module were 0.017 L/s and 0.03 L/s, respectively. The concentration of feed solution changed from 20000 ppm to 40000 ppm. Freshwater was used on permeate side, and the salinity of freshwater was under 100 ppm in all experiments (met the irrigation requirement criteria in Vietnam). For ensuring the reliable measured results, each experimental set was repeated three times.

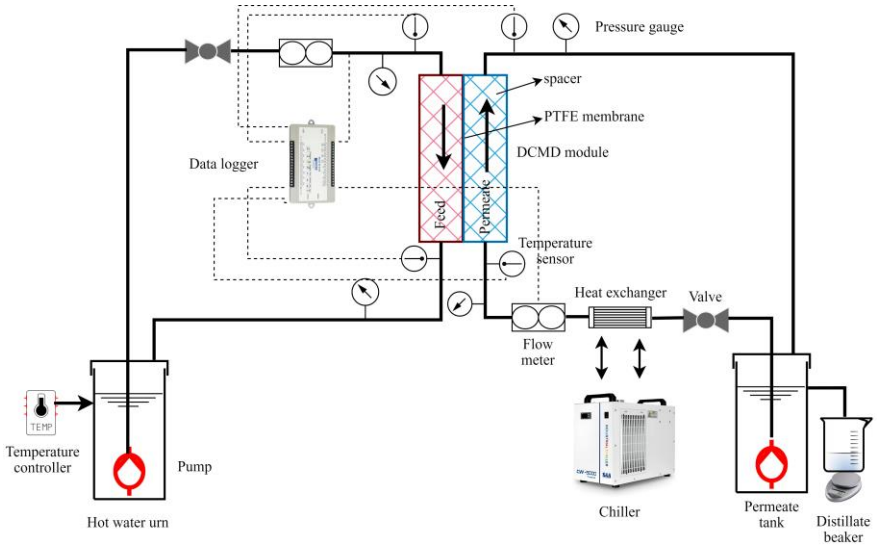

Figure 3. Experimental set-up

The uncertainties of experimental results were calculated by using The Taylor series method (TSM). The uncertainties of measurement devices were showed in Table 2, and the maximum uncertainty values of experimental mass fluxes were 0.0046 kg/m^2-h for PTFE022 membrane, and 0.0047 kg/m^2-h for PTFE045 and PTFE1 membranes.

Table 2. Uncertainties of experimental devices

Temperature sensor PT100	*± 0.5^{0}C*
Flow sensor (YF-S201)	*±10% of the reading*
Longitudinal dimensions	*±0.01mm*
Digital scale (weight)	*±0.1 g*
Time	*±0.2s*

For evaluating the accuracy of experimental mass fluxes and determining the most appropriate mass transfer model inside pores of membrane, the standard deviation (SD), the root mean square error (RMSE), and the mean absolute percentage error (MAPE) were also applied.

4. RESULTS AND DISCUSSIONS

4.1. Effect of Pore Size Of Membrane On Predicted Mass Fluxes Model Selection Under Different Operating Conditions

For the confirmation of the most appropriate mass transfer mechanism through pores of membrane, the experiments were carried out under effect of various experimental conditions, as described in Table 3. The nominal pore size of membranes varied from 0.22 µm to 1 µm.

Table 3. Experimental conditions for investigating the effect of pore size of membranes on mass fluxes in spacer-filled DCMD.

Experiment No.	T_{fi} (^{0}C)	T_{pi} (^{0}C)	$V_f = V_p$ (L/s)	S_f (ppm)
I.1	40	20	0.03	20000
I.2	45			
I.3; II.1; III.1	50			
II.2	50	20	0.017	20000
III.2	50	20	0.03	40000

The predicted mass fluxes implemented various mass transfer models described in

Table **1**. To determine the most suitable mass transfer model for membrane pores, two metrics, namely RMSE and MAPE, were utilized. It can be clearly seen that DGM could not be used to predict the mass fluxes in DCMD in all range of experimental membrane. In case of 0.22 µm PTFE membrane, all the mass transfer model except DGM could be applied to calculate the overall mass transfer coefficient through membrane pores, as shown in Figure 4 and Table 4. The large error of mass flux between experimental and DGM could be explained by the establishment of DGM depended on isothermal assumption, which was not suitable for DCMD configuration when thermal effect occurred across the transmembrane surface (non-isothermal system) [27]. These results were also coincident to other studies [18, 44] when the dependence of MD permeate mass flux on both feed and permeate temperature were confirmed.

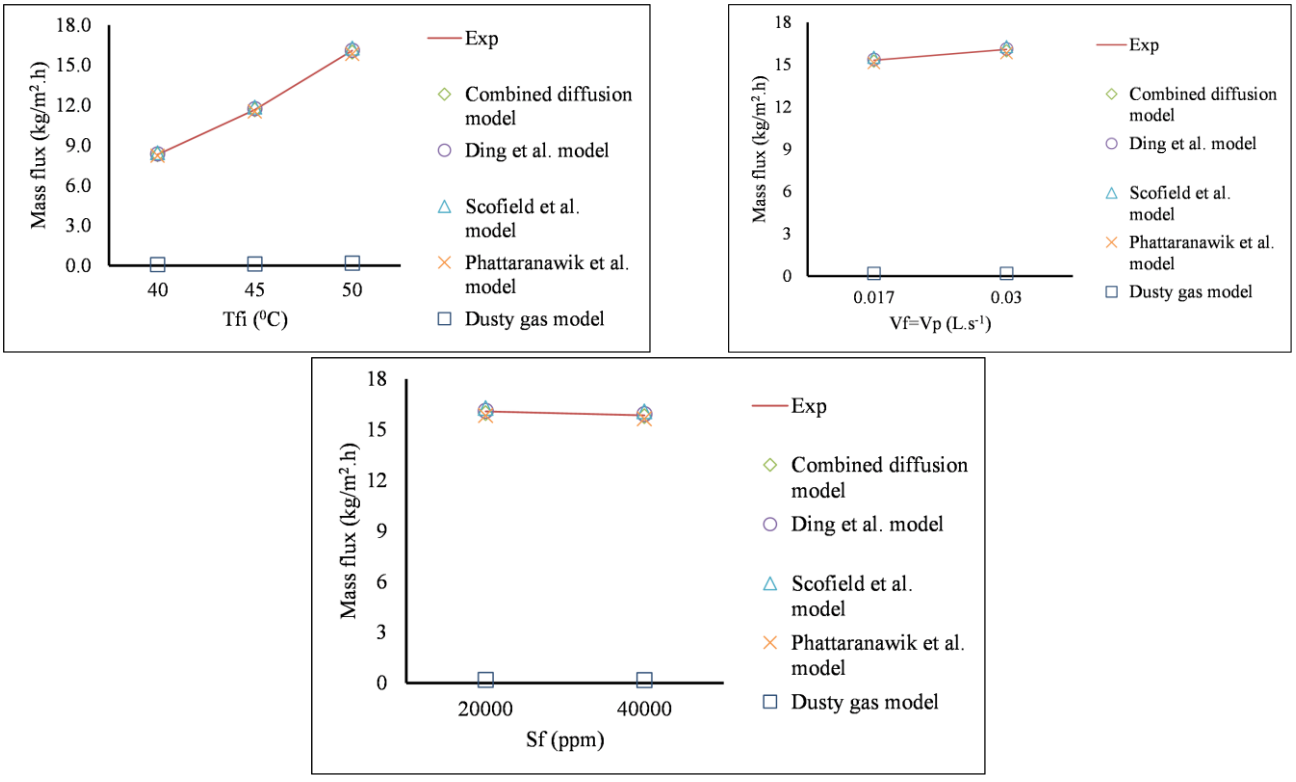

Figure 4. Experimental and predicted mass fluxes under effect of different experimental conditions in case of 0.22 µm pore size

Table 4. Estimating the dominant mass transfer model within membrane pores for 0.22µm commercial PTFE membrane

Parameters		Experimental No.				
		I.1	I.2	I.3, II.1, III.1	II.2	III.2
SD		0.125	0.193	0.280	0.154	0.095
RMSE	Combined diffusion model	0.26	0.22	0.40	0.43	0.50
	Ding et al. model	0.35	0.27	0.27	0.19	0.22
	Schofield et al. model	0.33	0.22	0.24	0.23	0.19
	Phattaranawik et al. model	0.39	0.27	0.34	0.28	0.36

	Dusty gas model	8.31	11.68	16.04	15.16	15.77
MAPE (%)	Combined diffusion model	2.15	1.52	1.84	1.83	2.28
	Ding et al. model	3.57	2.03	1.41	1.03	1.20
	Schofield et al. model	3.54	1.86	1.43	1.47	1.19
	Phattaranawik et al. model	4.05	2.07	2.03	1.74	2.13
	Dusty gas model	99.01	98.93	98.83	98.79	98.89

As illustrated in Figure 5 and Table 5, both mass transfer models proposed by Ding et al. [6] and Schofield et al. [13] obtained the best agreement between the calculated and measured mass fluxes for 0.45 µm PTFE membrane. The combined diffusion model and Phattaranawik et al. model could be also used, but the modelling results were less accurate with higher RMSE and MAPE values.

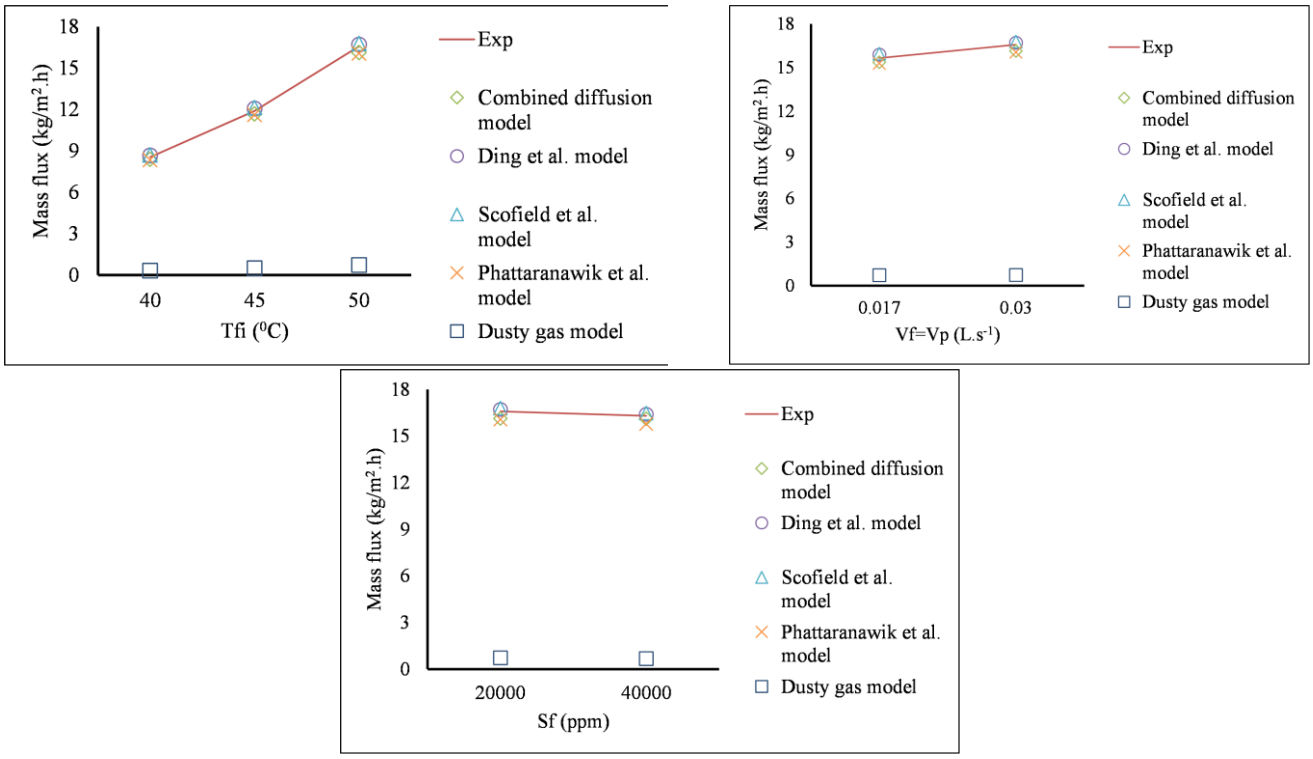

Figure 5. Experimental and predicted mass fluxes under effect of different experimental conditions in case of 0.45 µm pore size

Table 5. Estimating the dominant mass transfer model within membrane pores for 0.45µm commercial PTFE membrane

Parameters		Experimental No.				
		I.1	I.2	I.3, II.1, III.1	II.2	III.2
SD		0.125	0.122	0.171	0.218	0.197
RMSE	Combined diffusion model	0.27	0.22	0.55	0.47	0.51
	Ding et al. model	0.13	0.20	0.16	0.25	0.36
	Schofield et al. model	0.13	0.29	0.22	0.28	0.31
	Phattaranawik et al. model	0.37	0.34	0.68	0.62	0.73
	Dusty gas model	8.29	11.47	15.99	15.02	15.73
MAPE (%)	Combined diffusion model	2.82	1.76	3.16	2.49	2.41
	Ding et al. model	1.52	1.64	0.80	1.53	1.83
	Schofield et al. model	1.49	2.17	1.29	1.68	1.78
	Phattaranawik et al. model	3.74	2.77	3.59	3.57	3.99
	Dusty gas model	96.01	95.83	95.50	95.33	95.72

In case of 1µm PTFE membrane, it can be clearly seen that Poiseuille flow contributed a vital role to the overall mass transfer through membrane pores of membrane, as shown in Figure 6 and **Error! Reference source not found.**. The predicted mass fluxes from Ding et al. model and Schofield et al. model gave the best agreement with experimental mass fluxes in all investing conditions, while there was a larger difference between theoretical and

experimental results when combined diffusion model and Phattaranawik et al. model were implemented. While the maximum values of RMSE and MAPE for Ding et al. model and Schofield et al. model were 0.42 and 2.95%, these values for combined diffusion model and Phattaranawik et al. model were over 3 and 16.5%, respectively, as shown in **Error! Reference source not found.**.

Overall, the Poiseuille flow contributed insignificantly to overall mass transfer model when the pore size of membrane was not large enough, partially from 0.22 µm to 0.45 µm. However, the contribution of Poiseuille to the overall mass transfer was more considerable in case of larger pore size (1 µm).

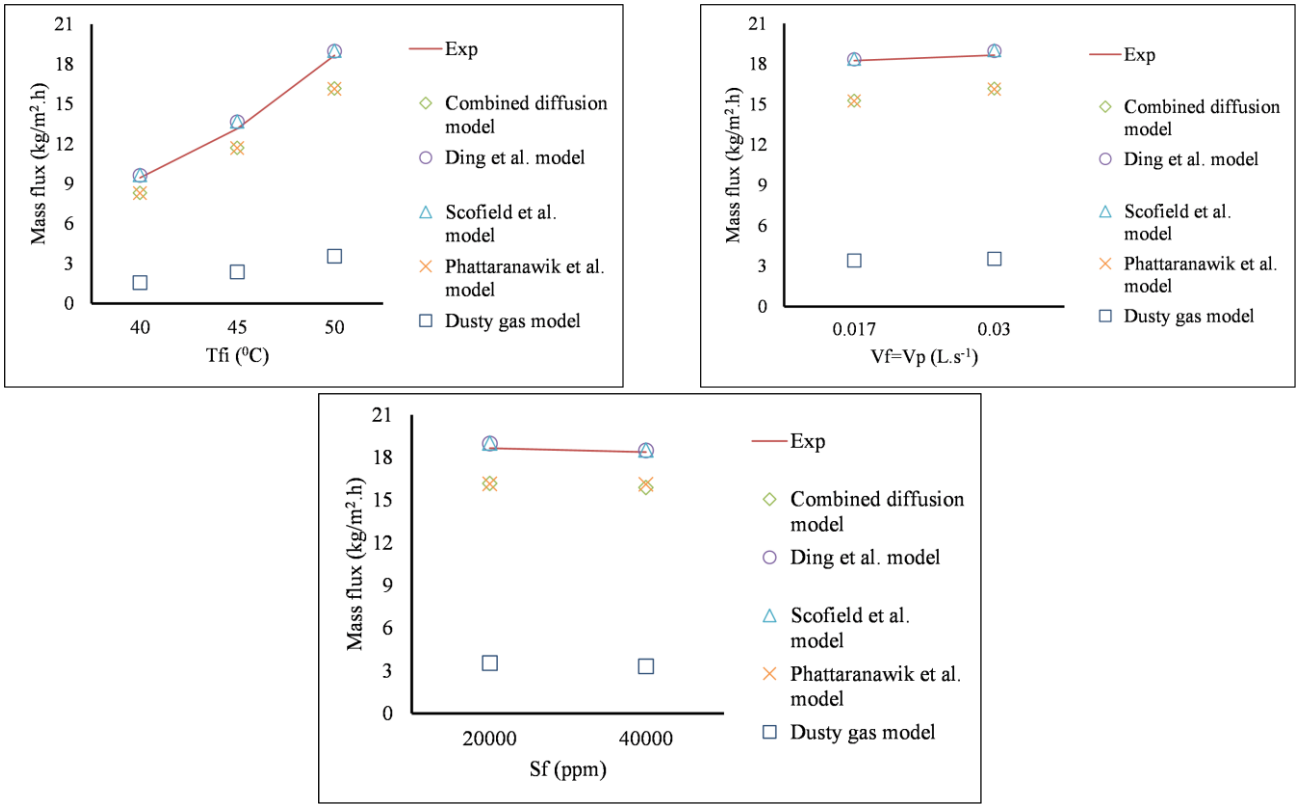

Figure 6. Experimental and predicted mass fluxes under effect of different experimental conditions in case of 1 µm pore size

Table 6. Estimating the dominant mass transfer model within membrane pores for 1 µm commercial PTFE membrane

Parameters		Experimental No.				
		I.1	I.2	I.3, II.1, III.1	II.2	III.2
SD		0.166	0.229	0.293	0.220	0.229
RMSE	Combined diffusion model	1.14	1.47	2.47	3.05	2.65
	Ding et al. model	0.15	0.39	0.27	0.06	0.13
	Schofield et al. model	0.16	0.42	0.31	0.08	0.16
	Phattaranawik et al. model	1.23	1.57	2.57	3.17	2.36
	Dusty gas model	7.84	10.86	15.15	14.96	15.02
MAPE (%)	Combined diffusion model	11.90	11.02	13.07	16.50	14.26
	Ding et al. model	1.42	2.72	1.28	0.26	0.69
	Schofield et al. model	1.59	2.95	1.62	0.32	0.86
	Phattaranawik et al. model	12.78	11.70	13.60	17.12	12.70
	Dusty gas model	81.67	81.43	80.31	80.95	80.90

4.2. Mass Transfer Mechanism In Pores Of Membrane

As demonstrated in the models presented in

Table **1**, in any flow mechanism, the temperature in membrane pores affected the membrane permeability (MP). The combined diffusion model and Ding et al. model was chosen to investigate whether or not the Poiseuille flow contribute to the mass transfer coefficient through membrane pores (or membrane permeability). In the experimental range of feed inlet temperature (T_{fi}) and experimental mass fluxes, the experimental MP values could be derived as shown in Figure 7. The feed inlet temperature varied from 40^0C to 50^0C with 5^0C increment, whereas 20^0C was the fixed permeate inlet temperature. The volume flowrates were kept equally in both feed and permeate side with 0.03 L/s. The feed concentration was 20000 ppm, and freshwater with salinity in the range of under 100 ppm was used in permeate side.

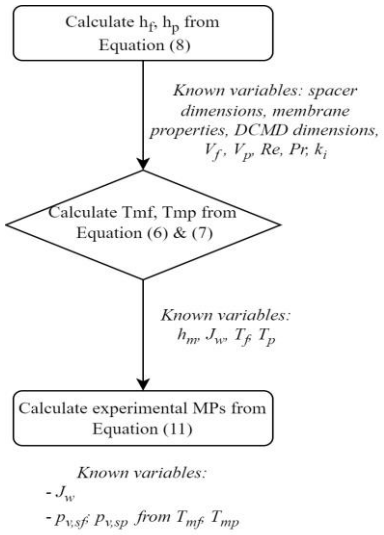

Figure 7. Estimating experimental MP values

The calculated and theoretical MP values based on two following methods: combined diffusion model and Ding et al. model under effect of different feed inlet temperature were described in Figure 8 for various pore size of commercial PTFE membranes, respectively.

As can be seen from Figure 8, the measured MP values increased trivial with increasing feed inlet temperature in both models. According to [6], the Knudsen-molecular transition could be implemented to illustrate the mass transfer mechanism in membrane pores. They showed that the measured MP values increased under 10% when the average membrane surface temperature (T_m) reached up to nearly 35^0C [6]. The same results were obtained in this study when the maximum difference of experimental MP values was only from 2.3% to 4% for three various nominal pore size of membranes including PTFE022, PTFE045, and PTFE1 in the estimated range of the average membrane surface temperatures being between 30^0C and 35^0C. However, the comparison between the theoretical and experimental MP may provide us more important information. From Figure 8, the difference between experimental and theoretical mass transfer coefficient in case of smaller membrane pore size (0.22 µm; 0.45 µm) in both models was insignificant. However, for 1µm membrane pore size, this difference became larger with nearly 16% for combined diffusion model, while the Ding et al. model gave a trivial difference (under 4%). Additionally, the fluctuation of MP value for PTFE1 membrane was larger than that for PTFE022, and PTFE045 membranes. As explained by Ding et al. [6], this difference may be attributed to Poiseuille flow. Obviously, the Poiseuille flow contributed a considerable role to the overall mass transfer mechanism in larger membrane pores (1µm), and this result was also proved by study of Damtie et al. [18]. When feed inlet temperature reached to 60^0C or 70^0C, Damtie et al. also showed inconsiderable increase with under 10% in MPs [18].

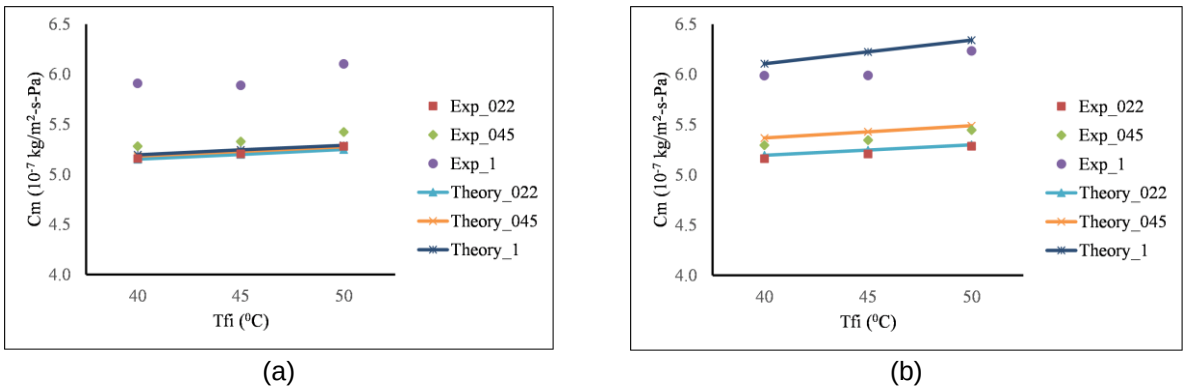

Figure 8. Experimental and theoretical membrane permeability values for different PTFE membranes according to (a) Combined diffusion model; (b) Ding et al. model.

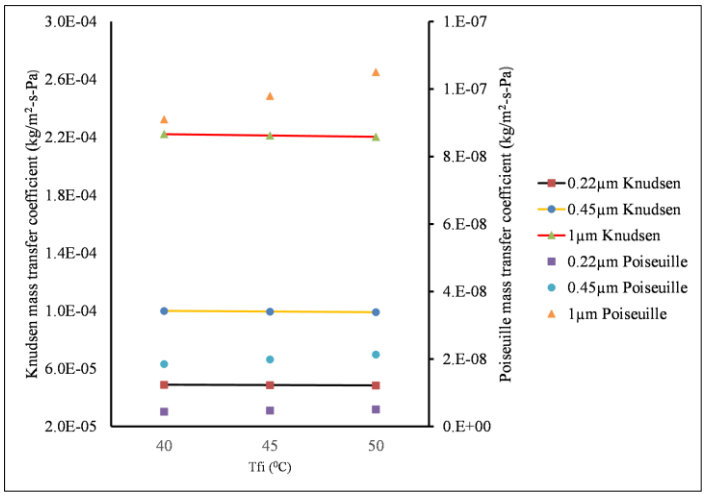

Figure 9. Knudsen and Poiseuille mass transfer coefficient regarding to feed inlet temperature for different membrane pore sizes implementing Ding et al. model.

It is no doubt that larger membrane pores obtained larger permeate fluxes in all range of experimental feed inlet temperatures, as shown in Figure 4, Figure 5 , and Figure 6. This result was due to the higher mass transfer coefficient (Figure 8) and thermal efficiency [18]. The increase of mass fluxes due to the leakage of feed solution through membrane to permeate side was also checked by measuring the salinity of freshwater production after each experimental run. All freshwater production obtained under 100 ppm of salinity. This meant there was no damage of membrane during experimental runs resulting in the error of experimental results. Additionally, the thermal efficiency was the ratio between evaporation of water molecules due to the latent heat and the total transported heat through the membrane [45]. As can be seen from Figure 4, Figure 5, and Figure 6, the mass fluxes were always higher for larger membrane pore size. As a result, the higher thermal efficiency was obtained for the larger membrane pore size.

As Figure 9 indicates that there was an insignificant decrease in Knudsen mass transfer coefficients as the feed inlet temperature increased across all the membrane ranges investigated. However, the fluctuation of Poiseuille mass transfer coefficient for 1μm PTFE membrane was more severe than that for smaller PTFE membrane in the same range of experimental temperatures. Consequently, the contribution of Poiseuille flow to the overall mass transfer model was more considerable in case of larger membrane pore size, and this conclusion was also proved through the better agreement of experimental and theoretical results in terms of mass fluxes and mass transfer coefficients when Ding et al. model was implemented in comparison to combined diffusion model.

CONCLUSIONS

The mass transfer behaviour within commercial PTFE membrane sample structure under the impact of different nominal pore sizes and operating conditions has been investigated experimentally and theoretically. With 0.22 – 1 µm nominal pore size of commercial PTFE membranes, the MP values increased insignificantly, with 2.3% and 4% when the T_{fi} increased from 40^0C to 50^0C (the inlet permeate temperature was kept at 20^0C). The Poiseuille flow mass transfer mechanism contributed considerably to overall mass transfer model in case of larger membrane pore size (1 µm), or in case of larger feed inlet temperature (although the overall mass transfer coefficient fluctuated insignificantly) [18]. The contribution of Poiseuille flow in Ding et al. model and Schofield et al. model was also reflected through the smallest MAPE and RMSE values in comparison to other investigated mass transfer models.

To sum up, based on this study's results, the role of the Poiseuille flow mechanism in mass flux prediction of PTFE 1µm membrane sample needs to be considered. For PTFE 0.22 µm and 0.45 µm membrane samples, all investigated mass transfer models except from Dusty Gas model could be responsible for the overall mass transfer prediction. DGM obtained the largest difference between experimental and predicted mass flux. This was due to the isothermal assumption of DGM that was not suitable for MD process when the thermal effect across membrane surfaces should be taken into account. Different membrane materials with larger nominal pore size (>1 µm) needs to be investigated further to have more adequate and accurate conclusions about the effect of membrane pore sizes on overall mass transfer mechanism within membrane pores.

Acknowledgement: This research was supported by HUE UNIVERSITY, grant number DHH2022-02-162.

Author Contributions: Conceptualization, Linh Ve and Farzaneh Mahmoudi; Investigation, Cuong Nguyen and Huy Nguyen; Methodology, Linh Ve, Cuong Do and Lich Nguyen; Software, Linh Ve and Tuan Hoang; Supervision, Linh Ve; Validation, Linh Ve, Cuong Do, Lich Nguyen and Farzaneh Mahmoudi; Visualization, Cuong Nguyen, Huy Nguyen and Tuan Hoang; Writing – original draft, Linh Ve; Writing – review & editing, Farzaneh Mahmoudi. All authors have read and agreed to the published version of the manuscript.

Conflicts of Interest: The authors declare no conflicts of interest.

Nomenclature

A	–	Membrane area, m^2
C_m	–	Membrane permeability, $kg.m^{-2}.s^{-1}.Pa^{-1}$
C_{km}	–	Membrane permeability for Knudsen-molecular diffusion mechanism, $kg.m^{-2}.s^{-1}.Pa^{-1}$
C_{kmv}	–	Membrane permeability for Knudsen-molecular-viscous flow, $kg.m^{-2}.s^{-1}.Pa^{-1}$
$\Delta H_{v,w}$	–	Vapour enthalpy of water, kJ/kg
J_w	–	Experimental mass flux, $kg.m^{-2}.s^{-1}$
M	–	Molecular weight of water, $kg.mol^{-1}$
MAPE	–	Mean absolute percentage error, %
P_a	–	Entrapped air pressure, Pa
P_m	–	Mean pressure within the membrane pores (or total pressure), Pa
Pr	–	Prandtl number
Q_f	–	Heat transfer rate through feed thermal boundary layer, W
Q_m	–	Heat transfer rate through the membrane, W
Q_p	–	Heat transfer rate through permeate thermal boundary layer, W
R	–	Gas constant, $J.mol^{-1}.K^{-1}$
Re	–	Reynolds number
RMSE	–	Root mean square error
S	–	Feed salinity, $g.kg^{-1}$
SD	–	Standard deviation
S_{vsp}	–	Specific surface of the spacer, m^{-1}
T_f	–	Bulk feed side temperature, K
$T_{f,i}$	–	Feed inlet temperature, K
T_m	–	Mean temperature at membrane surface, K
$T_{m,f}$	–	Temperature at the feed-membrane interface, K
$T_{m,p}$	–	Temperature at the permeate-membrane interface, K
T_p	–	Bulk permeate side temperature, K

$T_{p,i}$	–	Permeate inlet temperature, K
V_f	–	Volume flow rate at feed side, $L.s^{-1}$
V_p	–	Volume flow rate at permeate side, $L.s^{-1}$
W	–	Width of channel, m
d_f	–	Filament diameter, m
d_h	–	Hydraulic diameter in case of spacer-filled channels, m
d_p	–	Membrane pore diameter, m
h_f	–	Heat transfer coefficient at feed side, $W.m^{-2}.K^{-1}$
h_m	–	Heat transfer coefficient of the whole membrane, $W.m^{-2}.K^{-1}$
h_p	–	Heat transfer coefficient at permeate side, $W.m^{-2}.K^{-1}$
k	–	Thermal conductivity of water, $W.m^{-1}.K^{-1}$
k_B	–	Boltzman constant, $J.K^{-1}$
k_g	–	Thermal conductivity of gas phase, $W.m^{-1}.K^{-1}$
k_m	–	Thermal conductivity of membrane, $W.m^{-1}.K^{-1}$
k_p	–	Thermal conductivity of membrane material, $W.m^{-1}.K^{-1}$
l_m	–	Mesh size, m
$p_{v,sf}$	–	Partial pressure of water vapour at feed-membrane surface, Pa
$p_{v,sp}$	–	Partial pressure of water vapour at permeate-membrane surface, Pa
r	–	Mean pore size radius, m
t	–	Thickness of channel, m
t_s	–	Spacer thickness, m
Greek symbols		
τ	–	Membrane tortuosity
ε_m	–	Membrane porosity
ε	–	Spacer porosity
δ	–	Membrane thickness, m
θ	–	Angle between filaments of spacer, deg.
μ	–	Dynamic viscosity, $kg.m^{-1}.s^{-1}$
β	–	The reduced thermal polarizability
φ	–	Volume fraction of the dispersed phase (spheres)
Subscripts		
f	–	Feed
p	–	Permeate

REFERENCES

[1] Zarzoum, K.; M.M. Alquraish; K. Zhani; and H.B. Bacha. Experimental validation of membrane distillation unit coupled with direct contact membrane using solar energy. *Int. J. Low Carbon Technol.* **2023**, *18*, 542-553.

[2] Kujawska, A.; J.K. Kujawski; M. Bryjak; M. Cichosz; and W. Kujawski. Removal of volatile organic compounds from aqueous solutions applying thermally driven membrane processes. 2. Air gap membrane distillation. *J. Membr. Sci.* **2016**, *499*, 245-256.

[3] Fatima, S.; B. Govardhan; s. Kalyani; and S. Sridhar. Extraction of volatile organic compounds from water and wastewater by vacuum-driven membrane process: A comprehensive review. *Chem. Eng. J.* **2022**, *434*, 134664.

[4] Jiang, H.; A.P. Straub; and V. Karanikola. Ammonia Recovery with Sweeping Gas Membrane Distillation: Energy and Removal Efficiency Analysis. *ACS ES&T Engineering* **2022**, *2*, 617-628.

[5] Xie, Z.; T. Duong; M. Hoang; C. Nguyen; and B. Bolto. Ammonia removal by sweep gas membrane distillation. *Water Res.* **2009**, *43*, 1693-1699.

[6] Ding, Z.; R. Ma; and A.G. Fane. A new model for mass transfer in direct contact membrane distillation. *Desalination* **2003**, *151*, 217-227.

[7] Hitsov, I.; T. Maere; K. De Sitter; C. Dotremont; and I. Nopens. Modelling approaches in membrane distillation: A critical review. *Sep. Purif. Technol.* **2015**, *142*, 48-64.

[8] Dong, Y.; X. Dai; L. Zhao; L. Gao; Z. Xie; and J. Zhang. Review of Transport Phenomena and Popular Modelling Approaches in Membrane Distillation. *Membranes* **2021**, *11*.

[9] Ahadi, H.; J. Karimi-Sabet; M. Shariaty-Niassar; and T. Matsuura. Experimental and numerical evaluation of membrane distillation module for oxygen-18 separation. *Chem Eng Res Des* **2018**, *132*, 492-504.

[10] Mason, E.A. *Gas transport in porous media : the dusty-gas model*; Elsevier Science Ltd: Amsterdam, Netherlands, 1983; pp. 1-202.

[11] Khayet, M.; and T. Matsuura. *Membrane distillation: principles and applications*; Elsevier: Amsterdam, Netherlands, 2011; pp. 1-512.

[12] Schofield, R.W.; A.G. Fane; and C.J.D. Fell. Gas and vapour transport through microporous membranes. II. Membrane distillation. *J. Membr. Sci.* **1990**, *53*, 173-185.

[13] Schofield, R.W.; A.G. Fane; and C.J.D. Fell. Gas and vapour transport through microporous membranes. I. Knudsen-Poiseuille transition. *J. Membr. Sci.* **1990**, *53*, 159-171.

[14] Ismail, A.; and T. Matsuura. *Membrane Technology for Water and Wastewater Treatment, Energy and Environment*, 1st ed; CRC Press: London, England, 2016; pp. 1-388.

[15] Dahiru, U.L.; and E.K. Atia. Flux prediction in direct contact membrane distillation. *Int. J. Mater. Mech. Manuf.* **2014**, *2*, 302-308.

[16] Cath, T.Y.; V.D. Adams; and A.E. Childress. Experimental study of desalination using direct contact membrane distillation: a new approach to flux enhancement. *J. Membr. Sci.* **2004**, *228*, 5-16.

[17] Andrjesdóttir, Ó.; C.L. Ong; M. Nabavi; S. Paredes; A.S.G. Khalil; B. Michel; and D. Poulikakos. An experimentally optimized model for heat and mass transfer in direct contact membrane distillation. *Int. J. Heat Mass Transf.* **2013**, *66*, 855-867.

[18] Damtie, M.M.; Y.C. Woo; B. Kim; K.-D. Park; R.H. Hailemariam; H.K. Shon; and J.-S. Choi. Analysis of mass transfer behavior in membrane distillation: Mathematical modeling under various conditions. *Chemosphere* **2019**, *236*, 124289.

[19] Khayet, M.; A. Velázquez; and I. Mengual Juan. Modelling mass transport through a porous partition: effect of pore size distribution. *J. Non-Equil Thermody* **2004**, *29*, 279.

[20] Kim, Y.-D.; K. Thu; and S.-H. Choi. Solar-assisted multi-stage vacuum membrane distillation system with heat recovery unit. *Desalination* **2015**, *367*, 161-171.

[21] Manawi, Y.M.; M. Khraisheh; A.K. Fard; F. Benyahia; and S. Adham. Effect of operational parameters on distillate flux in direct contact membrane distillation (DCMD): comparison between experimental and model predicted performance. *Desalination* **2014**, *336*, 110-120.

[22] Manawi, Y.M.; M.A.M.M. Khraisheh; A.K. Fard; F. Benyahia; and S. Adham. A predictive model for the assessment of the temperature polarization effect in direct contact membrane distillation desalination of high salinity feed. *Desalination* **2014**, *341*, 38-49.

[23] Ve, Q.L.; R. Koirala; M. Bawahab; H. Faqeha; M.C. Do; Q.L. Nguyen; A. Date; and A. Akbarzadeh. Experimental investigation of the effect of the spacer and operating conditions on mass transfer in direct contact membrane distillation. *Desalination* **2021**, *500*, 114839.

[24] Ve, Q.L.; R. Koirala; M. Bawahab; H. Faqeha; M.C. Do; Q.L. Nguyen; A.S. Date; and A. Akbarzadeh. Theoretical modelling and experimental study of spacer-filled direct contact membrane distillation: Effect of membrane thermal conductivity model selection. *Desalination Water Treat.* **2021**, *217*, 63-11.

[25] Lawson, K.W.; and D.R. Lloyd. Membrane distillation. I. Module design and performance evaluation using vacuum membrane distillation. *J. Membr. Sci.* **1996**, *120*, 111-121.

[26] Schofield, R.W.; A.G. Fane; and C.J.D. Fell. Heat and mass transfer in membrane distillation. *J. Membr. Sci.* **1987**, *33*, 299-313.

[27] Lawson, K.W.; and D.R. Lloyd. Membrane distillation. *J. Membr. Sci.* **1997**, *124*, 1-25.

[28] Phattaranawik, J.; R. Jiraratananon; and A.G. Fane. Effect of pore size distribution and air flux on mass transport in direct contact membrane distillation. *J. Membr. Sci.* **2003**, *215*, 75-85.

[29] Triki, Z.; Z. Fergani; S. Lekmine; H. Tahraoui; A. Amrane; M. Zamouche; M. Kebir; A.A. Assadi; L. Khezami; and J. Zhang *Numerical Modelling and Performance Evaluation of Vacuum Membrane Distillation for Energy-Efficient Seawater Desalination: Towards Energy-Efficient Solutions*. Water, 2023. **15**, DOI: 10.3390/w15203612.

[30] Kalla, S.; R. Baghel; S. Upadhyaya; and K. Singh. Separation of HCl/water mixture using air gap membrane distillation, Taguchi optimization and artificial neural network. *Chem. Prod. Process. Model.* **2022**, *17*, 137-152.

[31] Suárez, F.; M.B. Del Río; and J.E. Aravena. Water Flux Prediction in Direct Contact Membrane Distillation Subject to Inorganic Fouling. *Membranes (Basel)* **2022**, *12*.

[32] Vanneste, J.; J.A. Bush; K.L. Hickenbottom; C.A. Marks; D. Jassby; C.S. Turchi; and T.Y. Cath. Novel thermal efficiency-based model for determination of thermal conductivity of membrane distillation membranes. *J. Membr. Sci.* **2018**, *548*, 298-308.

[33] García-Payo, M.C.; and M.A. Izquierdo-Gil. Thermal resistance technique for measuring the thermal conductivity of thin microporous membranes. *J. Phys. D Appl. Phys.* **2004**, *37*, 3008-3016.

[34] Phattaranawik, J.; R. Jiraratananon; and A.G. Fane. Heat transport and membrane distillation coefficients in direct contact membrane distillation. *J. Membr. Sci.* **2003**, *212*, 177-193.

[35] Ve, Q.L.; K. Rahaoui; M. Bawahab; H. Faqeha; A. Date; A. Akbarzadeh; M.C. Do; and Q.L. Nguyen. Experimental investigation of heat transfer correlation for direct contact membrane distillation. *J Heat Transfer* **2019**, *142*, 012001-1 - 012001-13.

[36] Da Costa, A.R. *Fluid Flow and Mass Transfer in Spacer-filled Channels for Ultrafiltration*; University of New South Wales: New South Wales, Australia, 1993.

[37] Ve, Q.L.; K. Rahaoui; M. Bawahab; H. Faqeha; A. Date; A. Faghih; and A. Akbarzadeh. An experimental heat transfer investigation of using spacer in direct contact membrane distillation. *Energy Procedia* **2019**, *160*, 223-230.

[38] Qtaishat, M.; T. Matsuura; B. Kruczek; and M. Khayet. Heat and mass transfer analysis in direct contact membrane distillation. *Desalination* **2008**, *219*, 272-292.

[39] Khayet, M.; M.P. Godino; and J.I. Mengual. Modelling transport mechanism through a porous partition. *J. Non-Equil Thermody* **2001**, *26*, 1.

[40] Nayar, K.G.; M.H. Sharqawy; L.D. Banchik; and J.H. Lienhard V. Thermophysical properties of seawater: a review and new correlations that include pressure dependence. *Desalination* **2016**, *390*, 1-24.

[41] Essalhi, M.; and M. Khayet, *10 - Fundamentals of membrane distillation*, in *Pervaporation, Vapour Permeation and Membrane Distillation*, A. Basile;A. Figoli; and M. Khayet, Editors. 2015, Woodhead Publishing: Oxford. p. 277-316.

[42] Khayet, M. Membranes and theoretical modeling of membrane distillation: a review. *Adv. Colloid Interface Sci.* **2011**, *164*, 56-88.

[43] Lawson, K.W.; and D.R. Lloyd. Membrane distillation. II. Direct contact MD. *J. Membr. Sci.* **1996**, *120*, 123-133.

[44] El Kadi, K.; K. Moustakas; and I. Janajreh. Comparison of different mass transfer models for direct contact membrane distillation flux evaluation. *Desalination Water Treat.* **2020**, *194*, 26-29.

[45] Khayet, M. Solar desalination by membrane distillation: dispersion in energy consumption analysis and water production costs (a review). *Desalination* **2013**, *308*, 89-101.

DOI: https://doi.org/10.15379/ijmst.v11i1.3623